arXiv:1607.07595v1 [astro-ph.GA] 26 Jul 2016

Exponential Disks from Stellar Scattering: III. Stochastic Models

Bruce G. Elmegreen[1], Curtis Struck[2]

ABSTRACT

Stellar scattering off irregularities in a galaxy disk has been shown to make an exponential radial profile, but no fundamental reason for this has been suggested. Here we show that exponentials are mathematically expected from random scattering in a disk when there is a slight inward bias in the scattering probability. Such a bias was present in our previous scattering experiments that formed exponential profiles. Double exponentials can arise when the bias varies with radius. This is a fundamental property of scattering and may explain why piece-wise exponential profiles are ubiquitous in galaxies, even after minor mergers and other disruptive events.

Subject headings: Galaxy:disk — Galaxies:evolution — Galaxies:structure

1. Introduction

The exponential shape for the radial profiles of galaxy disks (de Vaucouleurs 1959) has never been explained at a fundamental level. The initial mass and angular momentum distribution in the gaseous halo plays a role early-on (Eggen et al. 1962; Mestel 1963; Fall & Efstathiou 1980), as they lead to a nearly exponential shape during collapse if angular momentum is conserved (Freeman 1970). Numerical simulations confirm this result even with some redistribution of angular momentum (e.g., Dalcanton et al. 1997; Governato et al. 2007; Foyle et al. 2008; Sánchez-Blázquez 2009; Cooper 2013; Aumer & White 2013; Aumer et al. 2013; Stinson et al. 2013; Martig 2014; Herpich et al. 2015; Minchev et al. 2015; Rathaus et al. 2016). Initial conditions also seem involved for the far-outer gas disks of HI-rich galaxies, which have exponential profiles with a universal scale length when normalized to the radius where the HI surface density is 1 $M_\odot$ pc^{-2} (Wang et al. 2014). Bigiel & Blitz (2012) found a universal exponential gas profile when normalized to R_{25}, the radius at 25 magnitudes per square arcsec in the V band.

[1]IBM Research Division, T.J. Watson Research Center, P.O. Box 218, Yorktown Heights, NY 10598; bge@watson.ibm.com

[2]Department of Physics & Astronomy, Iowa State University, Ames, IA 50011; struck@iastate.edu

Disk stars also move radially after they form because of bulk motions in the presence of torques (Hohl 1971), guiding center migrations that preserve nearly circular orbits (Sellwood & Binney 2002; Roškar et al. 2008; Vera-Ciro 2014), and strong scatterings that make eccentric orbits (Bournaud et al. 2007). These motions can produce exponential profiles too. Numerical simulations show piece-wise exponentials after galaxy mergers (Younger et al. 2007; Borlaff et al. 2014; Athanassoula 2016), and galactic bars (Debattista et al. 2006) or bars coupled with spirals (Minchev et al. 2012) produce exponentials too. The bar and spiral profiles are consistent with observations of the locations of break radii between exponential segments, which tend to be at the outer Lindblad resonances of these patterns (Muñoz-Mateos et al. 2013; Laine et al. 2014). When there are no obvious perturbations, scattering off interstellar clouds and holes can still make exponentials (Elmegreen & Struck 2013; Struck & Elmegreen 2016), which are observed in dwarf Irregular galaxies too (Herrmann et al. 2013).

The underlying reason for exponential shapes in stellar scattering models has not been adequately investigated. This result was robust in our earlier papers, with exponential radial profiles appearing in two and three-dimensional models from initially uniform stellar distributions with randomly positioned scattering sites. The stellar particles were not self-gravitating so that spiral arms would be avoided, and a fixed potential for the orbits was assumed to avoid stellar momentum exchange with anything other than the scattering sites. These are the most basic ingredients for any disk model, so whatever drives evolution in them should also be present to some degree in more complete models.

Here we consider an interesting aspect of random scattering in a disk that may be relevant to the galaxy problem. This involves stochastic scattering with a slight inward bias, which always makes a radial profile that is essentially the same as an exponential. We also give evidence from our published scattering models that even though there was an overall expansion of the disk as the exponential grew in length, there was still a slight inward bias for each scattering event. Whether this model applies to real galaxies is not known, so we offer some observational tests for future research.

In what follows, Section 2 shows the change from a Gaussian to an exponential profile for one-dimensional scattering on a line when there is a biased probability toward the direction of a reflecting wall. Section 3 then considers two-dimensional scattering in a disk, which requires only the inward bias without the reflecting wall to make an exponential. Analytical models for these scattering profiles are in Section 4. Double exponentials as in Type II and III galaxies are discussed in Section 5. Section 6 shows the scattering bias in our previous 3D model for comparison with the stochastic theory. Section 7 offers some tests on the model. A summary is in Section 8.

2. Scattering along a Line

A convenient model for demonstrating the effects of scattering is a random walk along a line with steps to the left or right having certain fixed probabilities. Figure 1a shows a normalized histogram in red with the usual Gaussian shape made by scattering particles away from a starting point at $x = 30$ with an equal probability to the left ($q = 0.5$) and right ($p = 0.5$). The jumping distance per scatter is 0.5 units (see Sect. 4). The theoretically expected dispersion for this classical problem is $(Npq)^{0.5} = 2.73$ for $N = 30$ scatterings per point in this case. A theoretical Gaussian with this dispersion is shown superposed on the red histogram with a perfect fit. The number of particles used is 10^6, and the area is normalized to unity.

The blue histogram in Figure 1a shows another case with particles launched from $x = 30$ and $p = 0.5$, but now there are 300 scatterings per point, giving a larger dispersion. The green histogram is the same as the blue one but it has a bias to the left with $q = 0.55 > p = 0.45$. The bias moves the Gaussian to the left and shows no indication of the launching point, which is still at $x = 30$. Note that the Gaussian histograms cover both positive and negative x.

The shape of the histogram in Figure 1a changes significantly when there is a reflecting barrier in the direction of the bias. The magenta histogram shows a case like the green one, with 10^6 particles launched from $x = 30$ and a bias $p = 0.45$, but now there is a reflecting barrier at $x = 0$. That is, any particle that reaches $x = 1$ and is randomly directed toward the left is automatically returned to $x = 1$. The result of this reflection is to convert a Gaussian into an exponential. The scale length of the exponential is $1/\ln(q/p) = 4.98$, as derived in Section 4; a theoretical exponential with this scale length is shown by the straight magenta line, which runs parallel to the histogram, as expected. The jump distance in this case is 1 unit (see Sect. 4). The black histogram is made the same way as the magenta one, but with $p = 0.4$, which has a theoretical scale length of 2.466, as shown by the black line. Unlike the case for the Gaussians with no barrier, the exponentials do not change their shape as the number of scatterings per particle increases, once this number reaches a high enough value. Figure 1a has $N = 3000$ scatterings per particle for the two exponential cases. Increasing the number of particles affects all of the normalized histograms in the same way, by extending their reach to lower values on the ordinate (i.e., they go down to a value of $1/N$, at which point only one particle is present in the histogram bin.) Note that the launching point of $x = 30$ does not show up in the exponential profiles because they have reached an equilibrium shape at high N.

Figure 1b illustrates the development of the exponential for $p = 0.45$ as the number of scatterings per particle increases, all with 10^6 particles again. The step size is 0.5, as in the

Gaussians for figure 1a. For small numbers of scatterings per particle, the reflecting barrier is rarely sampled and a Gaussian histogram like the green one in Figure 1a appears. As each particle scatters more, the counts on the left climb up the barrier and the exponential appears. An explanation for this is in Section 4.

The black histogram with $p = 0.4$ in Figure 1a looks the same as the black histogram with $p = 0.45$ in Figure 1b although the two curves have different biases. This similarity is coincidental. The exponential cases in Figure 1a have unit steps for jumps in position, making equation (13) below relevant, while all cases in Figure 1b have half steps for the jumps in position to make a fair comparison with the green Gaussian in Figure 1a, which also has half-step jumps. When the step size is 0.5 unit, the scale length is half as much, as noted in the text below equation (13). Thus the scale length for the black histogram in Figure 1a is $1/\ln(0.6/0.4) = 2.466$ as mentioned above, and the scale length for the black histogram in Figure 1b is $0.5/\ln(0.55/0.45) = 2.492$, which is about the same.

3. Scattering in a Disk

3.1. Method

Scattering in a disk geometry involves the radial position of a particle and two angles, one for the particle position in the disk and another for the direction of scattering. We consider a circular coordinate system (r, θ) and some current position of a particle, (r_i, θ_i) (see Fig. 2). The particle is scattered for a unit distance $\lambda = 1$ in some direction α measured from the direction toward larger radii; α increases as the angle around the particle increases counter-clockwise.

This angle α is chosen with a bias toward the center of the coordinate system by picking a random number ζ between 0 and 1 and letting a generating angle α' be equal to $2\pi\zeta$, which means that α' is distributed uniformly. The actual scattering angle α is not distributed uniformly, but has an inward bias that comes from the generating angle α'. To generate this bias, we take

$$y = \sin(\alpha') \; ; \; x = \cos(\alpha') - b \tag{1}$$

for $b > 0$ a bias amount. The inwardly biased angle for next scattering is then

$$\alpha = \arctan(y/x). \tag{2}$$

The next radial position is determined from the triangle made by the current radial position and the scattering jump, using the trigonometric theory of cosines:

$$r_{i+1} = \sqrt{r_i^2 + \lambda^2 + 2\lambda r_i \cos(\alpha)}. \tag{3}$$

The next angular position in the coordinate system, θ_{i+1}, follows by first introducing the angle p from the trigonometric theory of sines, where

$$\sin(p) = \lambda \sin(\alpha)/r_{i+1} \tag{4}$$

and then

$$\theta_{i+1} = \theta_i + p. \tag{5}$$

The right-hand side of Figure 2 shows the distribution of scattering probabilities, $P(\alpha)$, as a function of the generating angle α' around the particle with $b = 0.1$. It is derived by setting $P(\alpha)d\alpha = P'(\alpha')d\alpha'$ with a constant distribution function for α', namely, $P'(\alpha') = 1/2\pi$. This gives $P(\alpha)$ in terms of α' from the derivative,

$$P(\alpha) = \frac{1}{2\pi}\frac{d\alpha'}{d\alpha} = \frac{1}{2\pi}\frac{1 - 2b\cos\alpha' + b^2}{1 - b\cos\alpha'}, \tag{6}$$

and then we convert α' into α for the value on the abscissa, as above. The dots in the plot are the equal intervals of α' used to evaluate $P(\alpha)$ for the figure. The probability is higher for $\alpha \sim \pi$, which corresponds to an inward direction.

3.2. Exponentials from an inward scattering bias

Figure 3 shows histograms of the radial positions of 315000 particles that follow from scattering in 2 dimensions with a bias ($b = 0.1$, see eq. (1)) directed toward the coordinate center $r = 0$. A histogram of azimuthal positions, θ, from equation (5) is flat because the particles scatter all over the disk (not shown). The launching radius ranges from 5 to 25 distance units, with the number of particles launched increasing linearly with distance, to mimic a constant surface density in this radial range. The resulting distribution is again exponential for a large number of scatterings per point because the origin of the coordinate system acts like a reflecting barrier. This is because points near the center that scatter toward smaller radius end up on the other side of the center at positive radius again. There is no imposed actual reflection, but just a natural impossibility of going to a negative radius. The four histograms in Figure 3 have different numbers of scatterings per particle. As the number increases, the exponential appears. The steepest exponential in the figure is essentially the equilibrium distribution; decreasing the number of scatterings from 3000 to 1000 (not shown) increases the scale length by only 3.8%.

Figure 4 shows normalized histograms of radial positions of a single particle that scatters various numbers of times from $N = 10^3$ to $N = 10^6$, always starting at a radial position $x = 5$ and with an inward bias of $b = 0.2$. As the number of scatterings increases, the limits

to the exponential become broader, but there is always about the same slope for small radii, converging to the theoretically predicted value for the assumed bias when N is sufficiently large. Note that the radial spread in the histograms is not from an outward bias, but simply from scattering multiple times.

4. Analytic Theory

4.1. Scattering on a line with no reflecting barrier

The widths and slopes of the equilibrium distributions of particle positions are derived here. Consider first a discrete model of scattering by fixed increments to the left or right on a line. The probability of scattering to the left is $q > 0.5$ and the probability of scattering to the right is $p < 0.5$, where $p + q = 1$. The distance of scattering is $1/2$ so the difference between the two possible scattered positions is 1, i.e., one cell width in a histogram. The cells alternate alignment along the half step and the full step. This is the standard model for a Galton box or bean machine (Trow 2007). We imagine that a new particle is introduced at position $i = 0$ at each time step, and that all existing particles at their integer positions i scatter to the left or right with these probabilities.

Without a reflecting barrier, the number of particles at position i after N steps is, on average, equal to the number in the previous step, $N - 1$, at position $i - 1/2$ times the probability that these particles scattered $1/2$ step to the right, which is p, plus the number in the previous step at $i + 1/2$ which scattered $1/2$ step to the left, which is q:

$$\Phi_N(i) = \Phi_{N-1}(i - 1/2)p + \Phi_{N-1}(i + 1/2)q. \tag{7}$$

In this case, i can be either positive or negative. Iterating this back to $N = 0$ on the right gives the usual result from the coefficients of the binomial expansion of $(p + q)^i$, which in the limit of large N and normalized to unit area is a Gaussian

$$\Phi_N(i) = \frac{1}{\sqrt{2\pi}Npq} \exp\left(-0.5(i/Npq)^2\right) \tag{8}$$

This explains the Gaussian distributions obtained above in the case of no reflecting barrier. The center of the Gaussian occurs at the cell position where the particles enter.

4.2. Scattering on a line with a reflecting barrier

With a reflecting barrier at $x = 0$ and with $q > p$, the probability distribution changes into an exponential. This may be seen in the same way by considering a particle introduced

at any position i at each time step and following the left or right scatterings of all existing particles, as above. The difference is that now the number at position $i = 0$ is the sum of the number in the previous step at $i = 0$ times the probability of a leftward motion, in which case the particle does not move at all because of the barrier, plus the number at $i = 1$ times the probability of a leftward motion,

$$\Phi_N(0) = \Phi_{N-1}(0)q + \Phi_{N-1}(1)q \tag{9}$$

All other probabilities, $\Phi_N(i)$, are as in equation (7) because they do not feel the barrier. A minor detail is that we take aligned cells now for each step so there is always a reflecting barrier at the lower end ($i = 0$), and we therefore take a unit length jump to the left and right. Thus we write in analogy to equation (7),

$$\Phi_N(i) = \Phi_{N-1}(i-1)p + \Phi_{N-1}(i+1)q. \tag{10}$$

Iterating Equation 9 back to the first step now gives a leading term $\Phi_N(0) = q^N$ and other terms multiplied by some combination of $q^k p^{N-k}$ for $k = 1$ to $N - 1$. This is because all counts $\Phi_N(i > 0)$ have to contain at least one product with p in order to get the particles somewhere to the right of $i = 0$. Similarly, one can derive the last term $\Phi_N(N) = p^N$. Experimentation with real examples readily shows that the distribution function $\Phi_N(i)$ has approximately equal factors (< 1) incrementing towards higher i, which means it is an exponential function. Taking just the endpoints, we derive the scale length as follows:

$$\ln \Phi_N(N) - \ln \Phi_N(0) = N \ln(p) - N \ln(q) = -N \ln(q/p) \tag{11}$$

or

$$\Delta \ln \Phi_N / \Delta i = -\ln(q/p) \tag{12}$$

which has the solution in the continuum limit for $0 \le i \le N$

$$\Phi_N(i) = \exp\left(-i \ln(q/p)\right). \tag{13}$$

Thus the exponential scale length is $1/\ln(q/p)$. Figure 1a has lines with slope of $-\ln(q/p)$, showing agreement between the stochastically determined histogram and this analytical result. Recall that without the barrier in the first example, we took alternately aligned cells with a half length jump. If we took a half length jump in the exponential case, the scale length would be half as large, $0.5/\ln(q/p)$. This is the case in Figure 1b to facilitate comparison with the non-reflecting distribution functions, i.e., the Gaussians, in Figure 1a.

4.3. Scattering in a disk

In a circular geometry, the number of particles in radial bins may be written as in equation (7), but the surface density is more important, and this involves a radial coordinate to keep track of the area in each radial interval. We introduce the surface density Σ and write the total number Φ as above with $\Phi \propto r\Sigma$. Knowing that the exponential reaches an equilibrium profile independent of the number of scatterings, N for large N (Sect. 2), we can write equation (7) as an equilibrium equation for the number of particles, considering an average step size λ for each scattering,

$$\Phi(r - \lambda/2)p = \Phi(r + \lambda/2)q \tag{14}$$

This equation states that at some position r, the number of outward jumps at probability p from a slightly smaller radius $r - \lambda/2$ equals the number of inward jumps at probability q from a slightly larger radius $r + \lambda/2$, per unit time. We let the excess probability of inward to outward scatterings be $\epsilon = q - p$. Setting $\Phi(r - \lambda/2) = \Phi(r) - 0.5\lambda d\Phi(r)/dr$ and the same for $\Phi(r + \lambda/2)$, equation (14) becomes

$$\frac{d\Phi(r)}{dr} = -\frac{2\epsilon}{\lambda}\Phi(r), \tag{15}$$

which has the solution

$$\Phi(r) = \Phi_0 \exp(-2\epsilon r/\lambda). \tag{16}$$

This is an exponential with a scale length of $r_{\rm D} = 0.5\lambda/\epsilon$.

We get the same result if we consider the scattering more carefully in two dimensions, using the angle α introduced above in equation (3). Then the balance between outward and inward scattering at position r is written,

$$\frac{1}{\pi}\int_{-\pi/2}^{\pi/2} \Phi(r - 0.5\lambda\cos\alpha)(1 - \epsilon\cos\alpha)d\alpha = \frac{1}{\pi}\int_{-\pi/2}^{\pi/2} \Phi(r + 0.5\lambda\cos\alpha)(1 + \epsilon\cos\alpha)d\alpha \tag{17}$$

which reduces to equation (15) and solution (16). This integral form considers all intermediate scattering angles. Note that the angle-dependent scattering probability given by equation (1) may be written approximately as $(1 - b\cos\alpha)/2\pi$, so $\epsilon \approx b$ in the present notation. Both of these expressions are not meant to reflect the actual scattering distribution function for real stars in a galaxy, but are the lowest order approximation to that function which preserves a directional bias.

The surface density Σ defined above is proportional to $\Phi(r)/r$, which varies as $e^{-r/r_{\rm D}}/r$ using $r_{\rm D} = 0.5\lambda/\epsilon$. For $r > r_{\rm D}$, this function becomes indistinguishable from an exponential with the same scale length. The inverse scale length in equation (16), 2ϵ, agrees fairly well

with the slope of the histogram in Figure 3, considering that $\lambda = 1$ in our discrete model. This slope is -0.187 outside $r = 10$ for inward bias $b = \epsilon = 0.1$ and $N = 3000$ scatterings per particle. For $b = 0.05$ (not shown in the figure) the slope is -0.113, and for $b = 0.2$, the slope is -0.388, both with $N = 3000$.

5. Double exponentials

Galaxy disks often show double exponential profiles with a downward bend at mid-radius for Type II and an upward band for Type III (e.g., Pohlen & Trujillo 2006). For Milky Way size disks, this bend could be the result of a change in stellar populations with old stars in the outer parts, as determined by color gradients (Bakos et al. 2008; Yoachim et al. 2012) or age gradients (Roediger et al. 2012; Ruiz-Lara et al. 2016). Age gradients are also present even in Type I disks, which suggests that stellar scattering is present in all disks. Because of these age gradients, the mass profiles can be a single exponential even if the light profile is Type II (Zheng et al. 2015). The average of a large number of light profiles at 3.6 μ, which is close to the mass profile at this wavelength, is a slightly down-bending double exponential (Muñoz-Mateos et al. 2013b).

Although there are reasonable dynamical models that can produce a double profile in the mass, purely stochastic scattering can do this too, making exponentials for each one, if there is a difference in the scattering bias for the inner and outer regions. If the outer part of a disk has a larger inward bias than the inner part, then the slope in the outer part will be steeper. A physical reason for this might be that the outer parts have only gas irregularities which scatter with an inward bias, while the inner parts have both gas irregularities with an inward bias plus spirals or bars with an outward bias from torques. Similarly, if the outer part of the disk has a smaller inward bias than the inner parts, perhaps because of weaker gas clumps in the outer parts, then the purely stochastic slope in the outer part will be shallower. In both cases, each segment will be approximately exponential because of the scattering process.

Figure 5 shows the results of scattering experiments in these two cases. Both histograms use 330000 particles with 1000 scatterings each. The particles are launched between radii of $r = 5$ and 10, with a number increasing linearly with radius to mimic a constant surface density. Both histograms also have a scattering bias from equation (1), $b = 0.1$, inside a radius of $r = 25$, but the blue histogram has $b = 0.2$ outside $r = 25$ while the red histogram has $b = 0.05$ outside $r = 25$. Each exponential is formed separately and locally, although the particles scatter over the disk. A gradually changing bias will produce a profile with more continuous curvature.

6. Numerical experiments

Elmegreen & Struck (2013) and Struck & Elmegreen (2016) ran simulations with non-self-gravitating test particles orbiting in a dwarf-irregular type galaxy potential with the addition of gravitational scattering centers from mass irregularities that are analogous to large clouds and holes in the interstellar medium. The test particles moved around in the disk because of the scattering and formed a stable exponential radial profile from an initially flat profile. We suspect that the exponentials in those papers have the same cause as the stochastic exponentials studied here, so we measured the scattering bias in the three-dimensional model of the second paper to see if it is directed inward.

Figure 6 illustrates this bias in two ways. The top panel shows the radius of all the stars at the end of the run on the ordinate versus their initial radius on the abscissa. The simulation time is 300 units, which equals 2.94 Gyr for a dwarf Irregular potential. The thick red line of equal initial and final radii separates the stars scattered to larger radii (above) and smaller radii (below). The thin black lines are offset by 2 radial units (1 kpc in physical units) from the red line. Most of the stars scattered outward lie between the red line and the upper black line. Many more stars are scattered inward, and a substantial fraction of them lie below the lower black line. Thus, more stars are scattered inward, and many of them are scattered farther inward than the outward scattering distance of stars scattered outward.

The lower panel of Figure 6 shows the distribution of the ratio of the final to initial radii from the top panel. The majority (64.5%) of the stars have values of this ratio less than unity, i.e., are scattered inward. Although not shown in these plots, this inward scattering fraction grows steadily with time and then saturates when the profile itself saturates to a fixed exponential once the disk gets thick. The black line in the lower panel is arbitrarily drawn (not a fit) to show the nearly linear form of the distribution to the left of the peak. The falloff to the right of the peak is steeper and nonlinear.

The 3D particle scattering model in Struck & Elmegreen (2016) is consistent with the essential features of the stochastic models described in this paper, namely the exponential equilibrium distribution of particle positions and the inward scattering bias. A plausible physical model for this bias is that initially circular orbits become more eccentric over time as stars scatter off of massive interstellar structures. The stellar energy hardly changes during such scattering because the structures are much more massive than each star. Eccentric orbits at fixed energy have less angular momentum than circular orbits, so the stars gradually lose angular momentum. That loss causes the inward bias. This situation differs from collective stellar motions induced by torques, such as the spreading of a disk outside the corotation radius of a bar or spiral, or in the presence of a companion galaxy. Those collective motions can give stars angular momentum, and they would presumably happen simultaneously with

the more energy-conserving scatterings off of interstellar structures. Stars are born in nearly circular orbits because the radial motions of the gas in which they form damp out. Eventually, stellar scattering decreases because the random motion and disk thickness get large. Then interactions with interstellar structures become too fast to deflect each star significantly, and too infrequent with the gas confined to the midplane to deflect each star very often. This saturation of the radial profile has the same origin as the usual explanation for the saturation of the stellar velocity dispersion (Lacey 1984). We see this saturation effect in our 3D simulations as well (Struck & Elmegreen 2016).

7. Model Tests

The stochastic scattering model for exponential profiles has little physical basis at the moment, and even if it operates in real galaxies, it may be overwhelmed by other processes and be difficult to see directly. The most direct test might be in other numerical simulations where small disk perturbations from gas structures or flocculent spiral arms scatter stars to different epicyclic guiding centers. Our prediction is that the distribution of the ratio of the guiding center radius after each scattering event to the radius before that event has a slight asymmetry toward values less than 1. That would confirm the assumption of an inward bias in scattering probability resulting from small perturbations. This is a different distribution function than the ratio of final to initial radius after many orbits, which will also contain bulk motions and resonant scattering off global spirals and bars. It is also different from the distribution function in the outer or inner parts of a disk, which will have a selection bias because most stars there scattered preferentially outward or inward to get to these positions.

An observational test might be provided by the far-outer regions of spiral galaxies, beyond the spirals where the disk gets relatively smooth. In two of the three galaxies observed by Watkins et al. (2016), the far-outer emission appeared to come from a disk rather than a halo of stars. These outer disk regions are still approximately exponential and yet there are no stellar features there like flocculent spiral arms that could scatter stars. Also in some low surface brightness galaxies there are no obvious spiral arms. A first test is if the stellar orbits are circular. Any gas that is present should have more circular orbits than stars because gas orbits cannot cross each other. If the stellar orbits are eccentric, then the rotation curve for the stars would be more declining in the outer parts than the gas. With both corrected for random motions via the asymmetrical drift correction, they should look the same. If the uncorrected gas and stars have the same rotation curves, then the stars are probably in circular orbits. For example, the low surface brightness galaxy eso-lv 2340130 in Pizzella et al. (2008) has a slightly lower rotation speed for the stars than

the gas, suggesting eccentric orbits for the stars. The effect should generally be small because frequent and weak stellar scatterings off of numerous, extended gas structures will not make highly eccentric orbits (Struck & Elmegreen 2016). Nevertheless, the test would involve mapping the column density and structure of gas in these spiral-free regions to see if there are significant perturbations from clouds, shells and holes. In the outer parts of disk galaxies and in low surface brightness galaxies, gravitational forces are relatively weak, relative orbital motions are slow, and cloud interaction timescales are long, so the required surface density irregularities in the gas can be small too and yet stellar scattering might have an important cumulative effect. If there is no gas in these regions and the stellar orbits are nearly circular, then something else might be scattering the stars locally, such as tiny satellite galaxies or dark matter mini-halos.

Exponential profiles in galaxies without gas clouds or other perturbations for stellar orbits would seem to be remnants of a former time when they had such scattering. Some S0 galaxies might be in this category.

The idealized stochastic model discussed here scatters particles all over the disk. Migration to outer galaxy disks is observed (Yoachim et al. 2012; Roediger et al. 2012; Ruiz-Lara et al. 2016), but the model also scatters particles to the inner disk, making an exponential profile from the outside in if there is initially a gap there. In real galaxies, several processes operating over a broad range of radii in the inner parts of disks could provide the reflection needed for the stochastic process. Then migrating stars need not get so close to the center. However, observations of stars in inner disks that migrated there from further out would be interesting.

8. Summary

Scattering of particles in 1 dimension produces the usual Gaussian distribution function when the particle can travel anywhere on the line, but this function changes to an exponential when there is a bias in the probability toward a reflecting barrier. The scale length of the exponential is $R_{\rm D} = 1/\ln(q/p)$ for inward and outward probabilities q and p and unit step size.

Scattering in 2 dimensions also produces exponential distribution functions in radius, or $\exp(-r/r_{\rm D})/r$ type functions which are nearly indistinguishable from exponentials, when there is an inward bias for each scattering event. Scattering can fill the whole disk out to very large radii even if the particles are launched from a narrow range of radii. The exponential reaches an equilibrium shape after a large enough number of scatterings per particle, with

a scale length of $R_{\rm D} = 0.5\lambda/(q-p)$ for scattering mean free path λ. Double exponentials analogous to galaxy profiles of Types II and III can be generated by varying the scattering bias over radius.

The scattering bias was determined from a previous three-dimensional numerical simulation (Struck & Elmegreen 2016) in which star particles scattered off of massive diffuse clouds in a dwarf galaxy potential. The simulation, which produced an exponential disk as shown in that paper, had an inward scattering bias shown here by the distribution of ratios of final to initial radii.

The scattering model may be relevant to the parts of galaxy disks that have been perturbed by interactions, accretion, ring formation, and other processes that change the average radial disk structure. Stellar scattering should gradually smooth over these irregularities, making them tend toward an exponential (or $e^{-r/r_{\rm D}}/r$) shape. Scattering should also change an initially tapered disk that forms by cosmological accretion into an exponential or piecewise exponential. The scattering bias assumed for the model is plausible because stars born in circular orbits that scatter elastically off massive clouds and other ISM structures lose angular momentum at nearly constant energy, which creates an inward bias.

REFERENCES

Athanassoula, E., Rodionov, S.A., Peschken, N. & Lambert, J.C. 2016, ApJ, 821, 90

Aumer, M. & White, S.D.M. 2013, MNRAS, 428, 1055

Aumer, M. & White, S.D.M., Naab, T., & Scannapieco, C. 2013, MNRAS, 434, 3142

Bakos, J., Trujillo, I., & Pohlen, M. 2008, ApJ, 683, L103

Bigiel, F. & Blitz, L. 2012, ApJ, 756, 183

Borlaff, A., Carmen Eliche-Moral, M., Rodríguez-Pérez, C., Querejeta, M., Tapia, T., Pérez-González, P.G., Zamorano, J., Gallego, J., & John Beckman, J. 2014, A&A 570, A103

Bournaud, F., Elmegreen, B.G., & Elmegreen, D.M. 2007, ApJ, 670, 237

Cooper, A.P., DSouza, R., Kauffmann, G., Wang, J., Boylan-Kolchin, M., Guo, Q., Frenk, C.S., & White, S.D.M. 2013, MNRAS, 434, 3348

Dalcanton J. J., Spergel D. N., Summers F.J., 1997, ApJ, 482, 659

Debattista V. P., Mayer L., Carollo C. M., Moore B., Wadsley J., & Quinn T., 2006, ApJ, 645, 209

de Vaucouleurs, G. 1959, ApJ, 130, 728

Eggen, O.J., Lynden-Bell, D., & Sandage, A.R. 1962, ApJ, 136, 748

Elmegreen, B.G., & Struck, C. 2013, ApJ, 775, L35

Fall S.M., & Efstathiou G. 1980, MNRAS, 193, 189

Foyle, K., Courteau, S., & Thacker, R. J. 2008, MNRAS, 386, 1821

Freeman, K. C. 1970, ApJ, 160, 811

Governato, F., Willman, B., Mayer, L., Brooks, A., Stinson, G., Valenzuela, O., Wadsley, J., & Quinn, T. 2007, MNRAS, 374, 1479

Herpich, J., Stinson, G.S., Dutton, A.A., Rix, H.-W., Martig, M., Roškar, R., Macciò, A.V., Quinn, T.R., & Wadsley, J. 2015, MNRAS, 448, L99

Herrmann, K.A., Hunter, D.A., & Elmegreen, B.G. 2016, AJ, 146, 104

Hohl, F. 1971, ApJ, 168, 343

Lacey, C. G. 1984, MNRAS, 208, 687

Laine, J., Laurikainen, E., Salo, H. et al. 2014, MNRAS, 441, 1992

Martig, M., Minchev, I. & Flynn, C. 2014, MNRAS, 442, 2474

Mestel L. 1963, MNRAS, 126, 553

Minchev, I., Famaey, B., Quillen, A. C., et al. 2012, A&A, 548, 127

Minchev, I., Martig, M., Streich, D., Scannapieco, C., de Jong, R.S., & Steinmetz, M. 2015, ApJL, 804, L9

Muñoz-Mateos, J.C., Sheth, K., Gil de Paz, A., et al. 2013, ApJ, 771, 59

Muñoz-Mateos, J.C., Sheth, K., Regan, M., et al. 2013b, ApJS, 219, 3

Pizzella, A., Corsini, E.M., Sarzi, M., Magorrian, J., Méndez-Abreu, J., Coccato, L., Morelli, L., & Bertola, F. 2008, MNRAS, 387, 1099

Pohlen, M., & Trujillo, I. 2006, A&A, 454, 759

Rathaus, B., & Sternberg, A. 2016, MNRAS, in press

Roediger, J.C., Courteau, S., Sánchez-Blázquez, P., & McDonald, M. 2012, ApJ, 758, 41

Roškar R.,Debattista, V. P., Stinson, G. S., Quinn T.R., Kaufmann T., Wadsley, J., 2008, ApJ, 675, L65

Ruiz-Lara, T.,Pérez, I., Florido, E. et al. 2016, MNRAS, 456, L35

Sánchez-Blázquez, P., Courty, S., Gibson, B.K., & Brook, C.B. 2009, MNRAS, 398, 901

Sellwood, J. A.., & Binney, J. J. 2002, MNRAS, 336, 785

Stinson, G.S., Bovy, J., Rix, H.W., Brook, C., Roškar, R., Dalcanton, J.J., Macciò, A.V., Wadsley, J., Couchman, H.M.P., & Quinn, T.R. 2013, MNRAS, 436, 625

Struck, C. & Elmegreen, B.G. 2016, submitted

Trow, P. 2007, http:ptrow.comarticlesGalton_June_07.htm

Vera-Ciro, C., DOnghia, E., Navarro, J., & Abadi, M. 2014, ApJ, 794, 173

Wang, J., Fu, J., Aumer, M., Kauffmann, G., Józsa, G.I.G., Serra, P., Huang, M.-l., Brinchmann, J., van der Hulst, T., Bigiel, F. 2014, MNRAS, 441, 2159

Watkins, A.E., Mihos, J.C., & Harding, P. 2016, arXiv605.05183

Yoachim, P., Roškar, R., & Debattista, V.P. 2012, ApJ, 752, 97

Younger, J.D., Cox, T.J., Seth, A.C., & Hernquist, L. 2007, ApJ, 670, 269

Zheng, Z., Thilker, D.A., Heckman, T.M. et al. 2016, ApJ, 800, 120

This preprint was prepared with the AAS LaTeX macros v5.2.

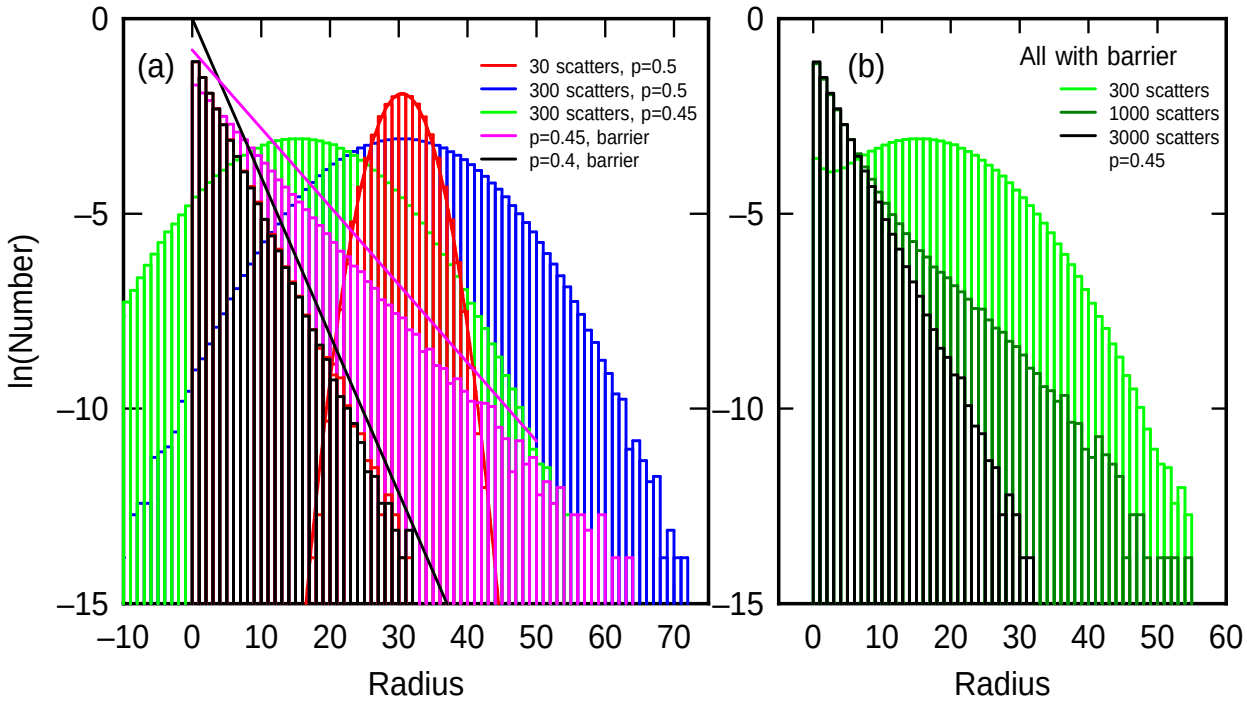

Fig. 1.— (a) One-dimensional distribution of 10^6 particles launched from position 30 and scattered $N = 30$ times (red) and 300 times (blue) with equal probabilities of scattering to the left ($q = 0.5$) and right ($p = 0.5$). The red histogram has a superposed Gaussian with the theoretical dispersion $(Npq)^{0.5}$. The distribution shifts to the left (green) when there is a bias in scattering that direction, using $p = 0.45$ and $q = 0.55$. The magenta and black distributions also launch particles from position 30 but they have a reflecting barrier at position 0, which turns the Gaussian shape into an exponential. There are $N = 3000$ scatterings per particle in these two cases. The step size for the scattering without a reflecting barrier is 1/2 unit, and the step size for scattering with a reflecting barrier is 1 unit. The scale length of the exponential is $1/\ln(q/p)$ in this case (Eq. 13), as indicated by the lines running offset and parallel to the histograms. (b) Steps in the development of an exponential for $p = 0.45$ as the number of scatterings per particle increases from 300 to 1000 to 3000. The step size is 1/2 unit, as for the non-reflective cases in (a).

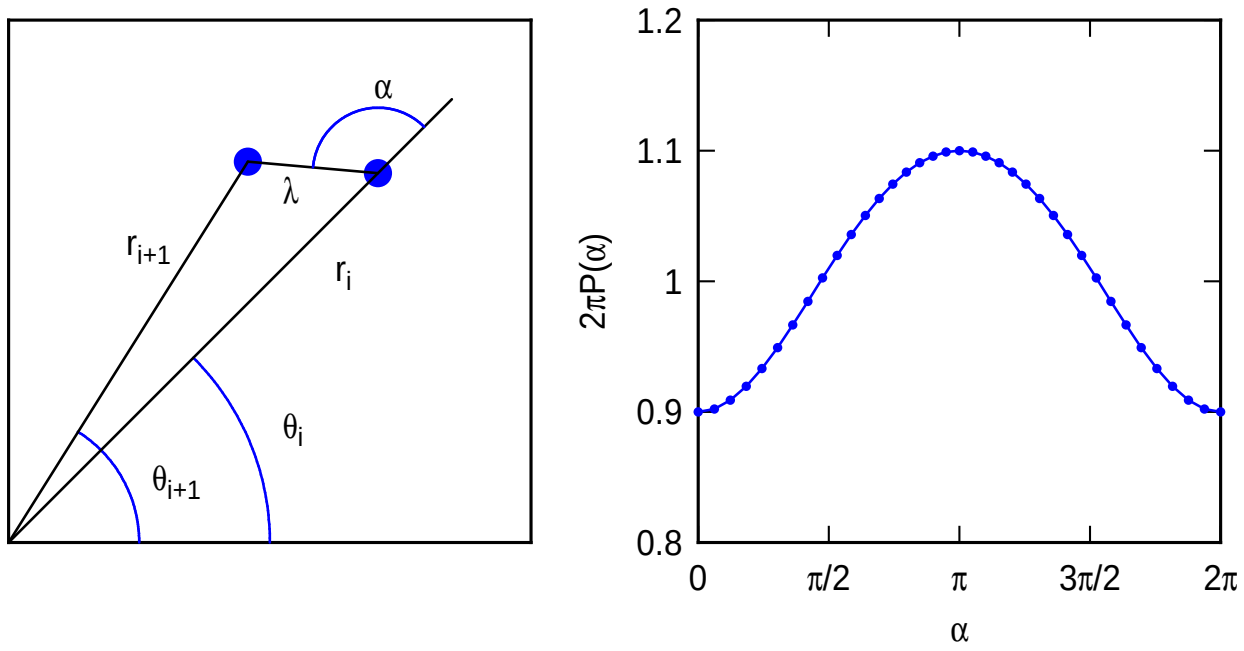

Fig. 2.— (left) Nomenclature for radii and angles in the two-dimensional scattering experiments. The particle scatters from position i to $i+1$. (right) Distribution function of the scattering angle α showing a bias with $b = 0.1$ toward the center of the coordinate system ($\alpha = \pi$).

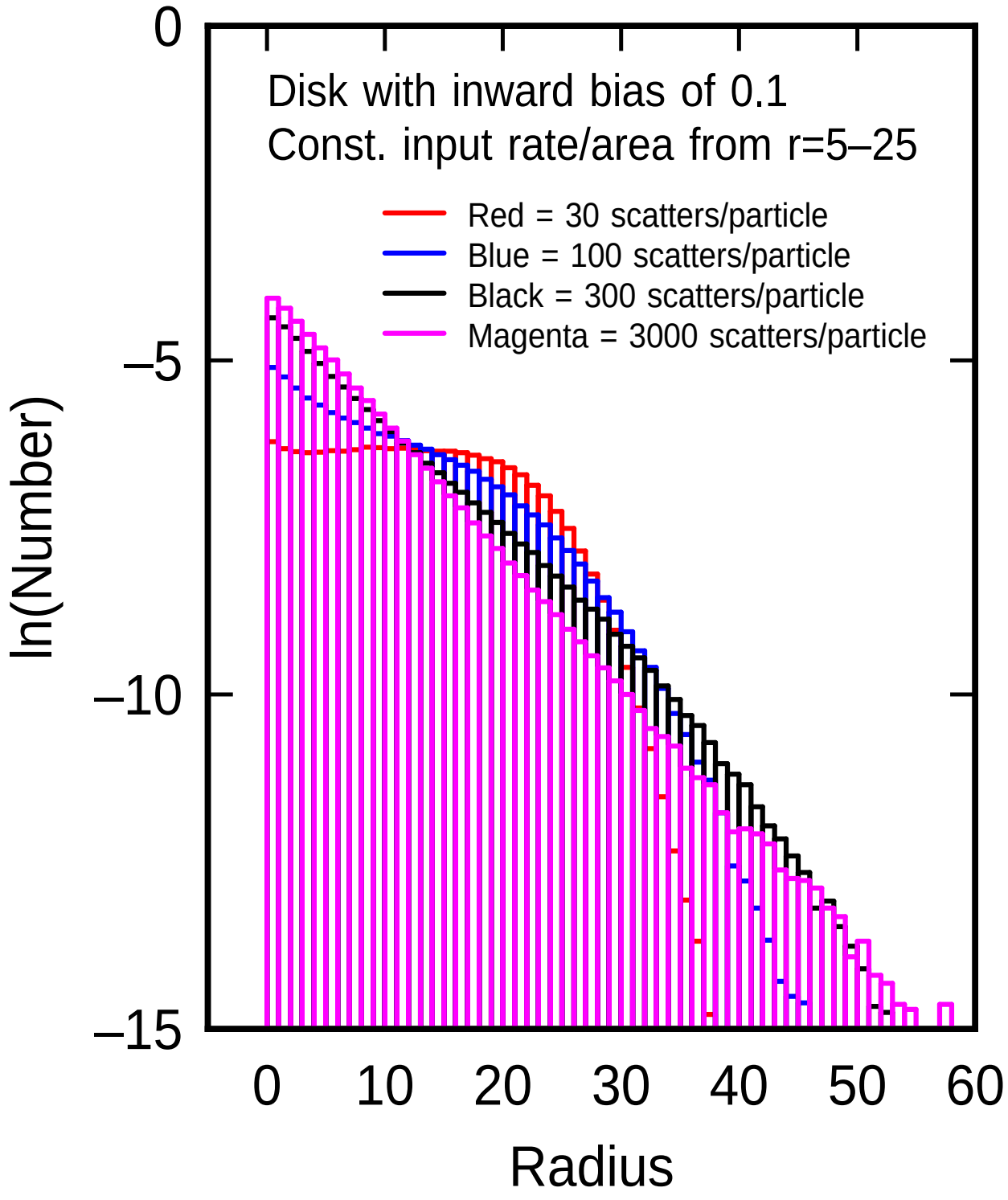

Fig. 3.— Scattering in a disk with increasing number of scatterings per particle in the 4 histograms showing convergence to an exponential radial profile. Particles are launched with a uniform rate per unit area from a radius of 5 to a radius of 25. A slight inward bias is imposed on the scattering angle with the parameter $b = 0.1$.

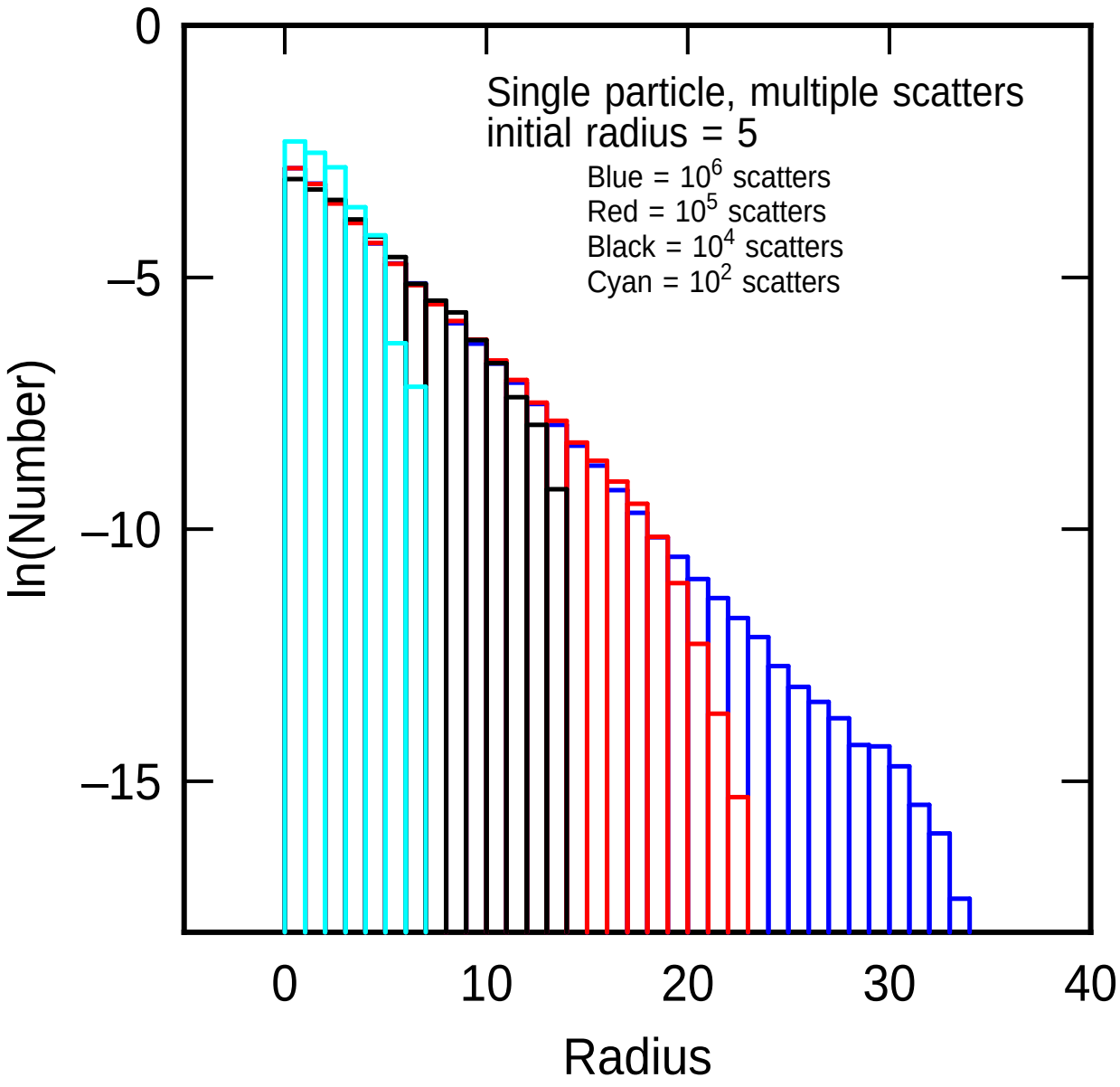

Fig. 4.— Four distribution functions show the positions occupied by a single particle that scatters a various number of times from 10^2 (cyan) to 10^6 (blue). Each case starts with a particle at a radius of 5 and has an inward bias given by $b = 0.2$. As the number of scatterings increases, the distribution function of radii covered by that particle broadens but maintains a fixed exponential slope for small radii, which are well sampled.

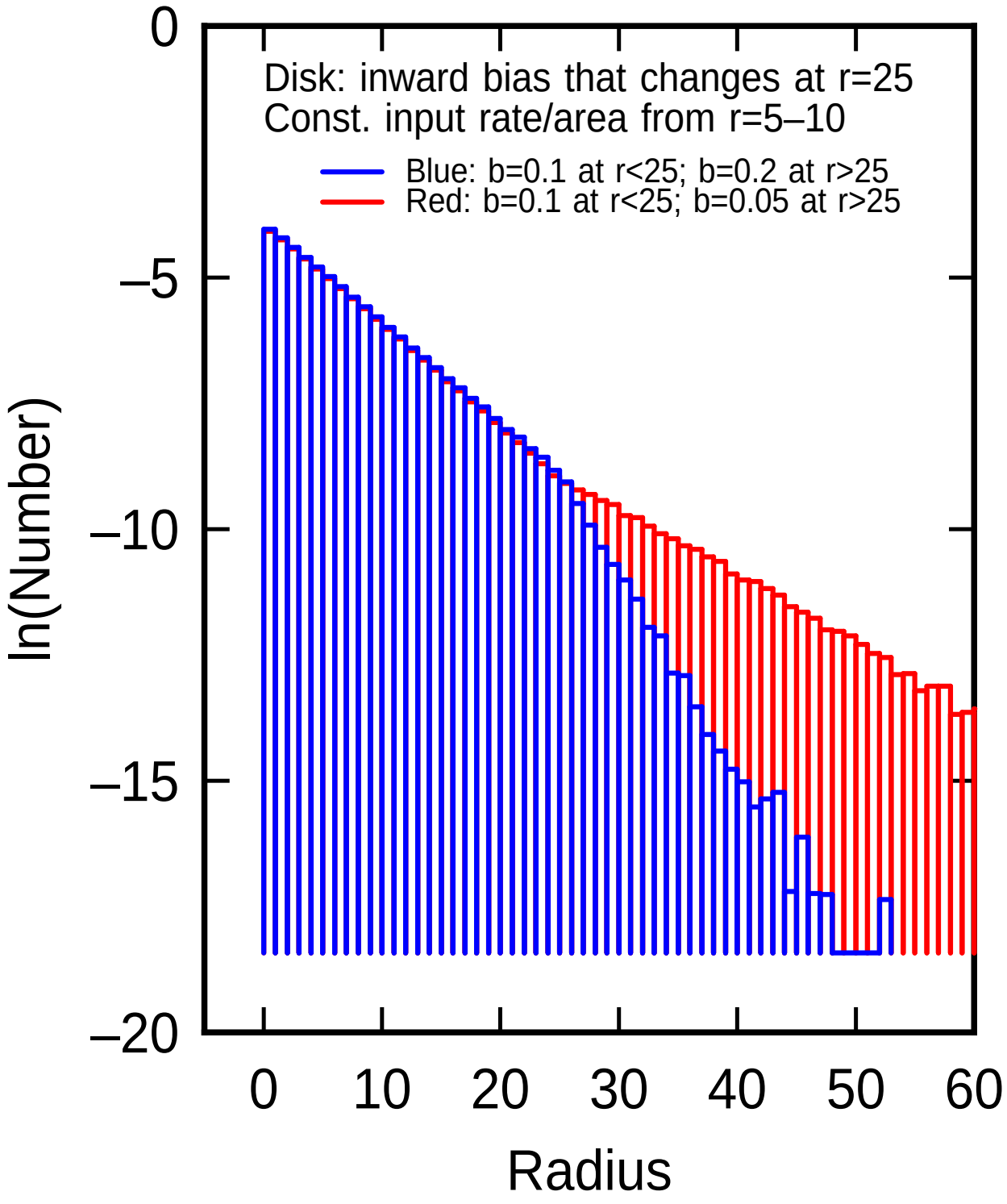

Fig. 5.— Double exponentials made from scattering 330,000 particles launched with a uniform surface density between radii of 5 and 10, and with 1000 scatterings per particle. Both histograms have an inward bias of $b = 0.1$ for radii less than 25. The red and blue histograms have smaller, $b = 0.05$, and larger, $b = 0.2$, inward biases outside that radius, producing double exponential forms of Types III and II, respectively.

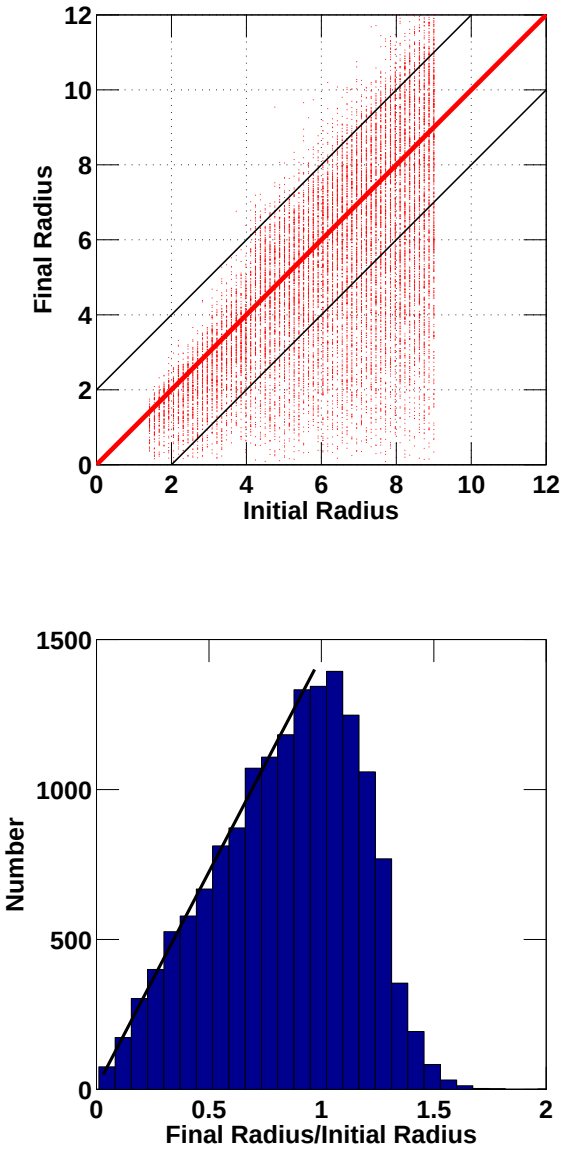

Fig. 6.— (Top) The initial versus final radii of 15,600 particles in a three-dimensional simulation with a dwarf galaxy potential and star particles scattering off of massive clouds (Struck & Elmegreen 2016). The simulation was run for 300 time units (2.94 Gyr). The thick red line denotes equal initial and final radii, while the thin black lines are offset by 2 radial units (1 radial unit equals 0.5 kpc). (Bottom) The distribution of the values of the ratio of final to initial radii in that simulation. A total of 64.5% of the particles had a ratio of radii less than 1.0, indicating that an inward scattering bias naturally occurred in the model. The black line suggests that the distribution function for this ratio increases approximately linearly as the ratio increases from 0 to 1.0.